Screening Linear and Circular RNA Transcripts from Stress Granules

Shuai Chen[1,2,#], Jinyang Zhang[1,#], Fangqing Zhao[1,2,3,4,*]

[1]*Beijing Institutes of Life Science, Chinese Academy of Sciences, Beijing 100101, China*

[2]*University of Chinese Academy of Sciences, Beijing 100049, China*

[3]*Center for Excellence in Animal Evolution and Genetics, Chinese Academy of Sciences, Kunming 650223, China*

[4]*Key Laboratory of Systems Biology, Hangzhou Institute for Advanced Study, University of Chinese Academy of Sciences, Hangzhou 310013, China*

[#] Equal contribution.

[*] Corresponding author.

E-mail: zhfq@biols.ac.cn (Zhao F).

Runing title: *Chen S et al / Liner and Circular RNAs in Stress Granules*

Total word counts: 3031.

Total references: 39.

Total figures: 3.

Total supplementary figures: 1.

Total supplementary tables: 4.

Total letters in the article title: 58.

Total letters in the running title: 46.

Total keywords: 5.

Total words in Abstract: 136.

Abstract

Stress granules (SGs) are cytoplasmic ribonucleoprotein assemblies formed under stress conditions and are related to various biological processes and human diseases. Previous studies have reported the regulatory role of some proteins and linear RNAs in SG assembly. However, the relationship between circular RNAs and SGs has not been discovered. Here, we screened both linear and circular RNAs in SGs using improved total RNA sequencing of purified SG cores in mammalian cells and identified circular transcripts specifically localized in SGs. Circular RNAs with higher SG-related RBP binding abilities are more likely to be enriched in SGs. Furthermore, some SG-enriched circular RNAs are differentially expressed in hepatocellular carcinoma and adjacent tissues. These results suggest the regulatory role of circular RNAs in SG formation and provide insights into the biological function of circular RNAs and SGs in hepatocellular carcinoma.

Keywords: Stress granule; Circular RNA; Protein–RNA interaction; RNA-seq; Hepatocellular carcinoma

Introduction

Stress granules (SGs) are membrane-less condensates that are dynamically and reversibly formed with ribonucleoproteins by phase separation [1]. SGs usually assemble in response to stress conditions [2]. Recent studies have shown that SGs are associated with cellular biological processes and various human diseases, such as degenerative diseases and malignant tumors [3–5]. Some RNA-binding proteins (RBPs) like Ras GTPase-activating protein-binding protein (G3BP), TIA-1, and TAR, are proved to be essential in SG assembly, and G3BP1 serves as the core component of SGs [6–8]. In addition to proteins, RNAs are associated with SG formation as well. A fraction of translationally proceeded or arrested mRNAs is localized in SGs [9,10]. Moreover, the principle of mRNA and noncoding RNA (ncRNA) accumulation in SGs are revealed in the transcriptome of SG cores [11]. However, these studied SG-related RNAs are all linear transcripts. Circular RNAs (circRNAs) specifically recruited to SGs have not been elucidated.

To address this issue, we improved the purification and sequencing approach of total RNAs in SG and screened circRNAs in SGs from the transcriptome of purified SG cores induced from mammalian cells. We identified 130 SG-enriched circRNAs and 2462 SG-depleted circRNAs, which revealed the specific accumulation of circRNAs in SGs. The circRNAs enriched in SGs exhibit stronger ability to interact with SG-related RBPs, even the SG core component G3BP2. In addition, some SG-enriched circRNAs are differentially expressed in hepatocellular carcinoma (HCC) and adjacent tissues, indicating the potential role of circRNAs and SGs in HCC.

Results

RNA transcripts enriched in SG cores

To determine the transcriptome of SG cores, we isolated total RNAs from purified SG cores in triplicates from SMMC-7721 cells, followed by RNA-seq analysis (**Figure 1**A). Since only few SGs formed in cells grown under normal conditions, we induced

SGs by incubating cells with 0.5 mM $NaAsO_2$ for 1 h. Immunofluorescence (IF) analysis of G3BP1 protein identified cytoplasmic SG condensates after stimulation (Figure 1B). Then, SGs were separated from cell lysates by differential centrifugation and purified by immunoprecipitation (IP) with G3BP1-specific antibodies. Western blot analysis of IP products showed that the SG core component G3BP1 and another SG associated protein CAPRIN1 could be enriched by specific antibodies (Figure 1C). For each sample, RNA was isolated for RNA-seq from purified SGs, 5% of cell lysates, and the supernatants without SGs of the IP solution, which are referred to as SG-RNA, total-RNA, and sup-RNA, respectively (Figure 1A).

Pairwise correlation analysis of the transcriptomes of the three RNA groups demonstrated the high reproducibility between experimental replicates in the same group ($R^2 > 0.9$; Figure 1D). Moreover, both SG-RNA and sup-RNA transcriptomes showed low correlations with total-RNA transcriptomes ($R^2 < 0.5$), suggesting that SG-RNA transcriptomes are different from total-RNA transcriptomes. In addition, principal component analysis (PCA) also highlighted the similarities within each transcriptome triplicates of SG-RNA, total-RNA, and sup-RNA as well as the differences between these three RNA groups (Figure 1E). Therefore, these findings demonstrated that SGs contain specific transcriptomes compared with cytosolic total RNAs and the RNAs outside of SGs.

SG-enriched RNAs are longer and have higher GC content

Since there were differences between the transcriptomes of SG-RNA, sup-RNA, and total-RNA, we thought to identify the specific transcripts that are enriched or depleted in SGs. According to the general analysis of RNA profiles in these transcriptomes, more fraction of mRNA transcripts was detected in SG-RNA than in total-RNA and sup-RNA, while long noncoding RNA and circRNA transcripts were fewer (**Figure 2**A, Table S1), indicating the translation regulation roles of SGs. Furthermore, differential expression analysis indicated that 1413 transcripts were significantly

enriched in SGs, while 4577 transcripts were significantly depleted in SGs compared with total-RNA and sup-RNA groups (adjusted $P < 0.05$) (Figure 2B). RNA fluorescence *in situ* hybridization (FISH) of two SG-enriched genes, *ANKRD11* and *COL7A1*, together with IF showed that both RNAs were colocalized with SGs (Figure 2C). GO analysis for SG-enriched and SG-depleted transcripts showed that the SG-enriched transcripts were involved in regulating RNA transcription, while the SG-depleted transcripts were associated with membrane targeting of proteins (Figure 2D). These findings demonstrated the transcription regulation role of SGs, which was supported by previous study [12], as transcription of most genes is inhibited under stress conditions. We also examined the molecular features of RNAs in SGs. The SG-enriched RNAs tended to be longer (2267 nt versus 1252 nt on average) and had higher GC content than SG-depleted RNAs (Figure 2E and F).

SG-enriched circRNAs have stronger ability to bind SG-related RBPs

As increasing studies have highlighted the importance of circRNAs in various biological processes, we further used the CIRI software [13–16] to identify and quantify the circRNAs that were recruited to SGs. According to the differential expression analysis, 130 circRNAs were significantly enriched in SGs, while 2462 were significantly depleted in SGs ($P < 0.05$) (**Figure 3**A). Among the enriched circRNAs, 66 have the sequence and annotation information in the circAtlas database [17,18] (Table S2). We also validated the localization of two circRNAs, *circSLTM* and *circARHGAP5*, in SGs by RNA FISH and IF (Figure 3B).

To uncover the characteristics of enriched circRNAs in SGs, we performed analysis on the sequence features and molecular functions of these circRNAs. Although longer mRNA transcripts tended to be enriched in SGs (Figure 2E), SG-enriched circRNAs (average length = 413 nt) were significantly shorter compared with SG-depleted circRNAs (average length = 537 nt) ($P < 0.001$, Wilcoxon test) (Figure 3C). In addition, there was no significant difference in GC content between

SG-enriched and SG-depleted circRNAs (Figure 3D), indicating that GC content was not associated with SG accumulation of circRNAs. Given that RNAs that bind more SG-related RBPs are more likely to be localized into SGs, whether SG-enriched RNAs exhibit higher RBP binding ability were evaluated. RBP binding sites prediction by RBPmap web server [19] found that there was no significant difference in types of RPBs between SG-enriched RNAs and SG-depleted RNAs (Figure 3E). However, SG-enriched circRNAs could bind fewer types of RBPs than SG-depleted circRNAs (Figure 3F). Surprisingly, we observed that the proportion of binding sites of SG-related RBPs were higher in SG-enriched RNAs than SG-depleted RNAs (Figure 3G), as well as in circRNAs (Figure 3H). Furthermore, analysis of the top 15 RBPs with higher binding density on SG-enriched circRNAs showed that most of them were SG-related RBPs (Figure 3I). Among them, G3BP2 was a core component of SGs, indicating the role of circRNAs in regulating SG formation. Taken together, these results demonstrate that circRNAs with higher capability of binding SG-related RBPs show a stronger preference to be recruited into SGs and circRNAs are involved in the formation of SGs through binding to their component proteins.

Differentially expressed SG-enriched circRNAs in HCC

Previous studies demonstrate that SGs are associated with human diseases like cancer [20]. We further examined whether there are SGs-enriched circRNAs associated with HCC, since the SG transcriptomes were purified from HCC cells. We screened 35 SG-enriched circRNAs that were expressed in HCC and adjacent tissues, and found three circRNAs, *circEXOC6B*, *circCALD1*, and *circVAMP3* that were significantly down-regulated in HCC tissues (Figure S1). These results indicate the potential roles of mutual interplay between these circRNAs and SGs in HCC.

Discussion

Assembly of SGs can be influenced by stress stimulation, as well as regulated by proteins and RNAs. RBPs are reported to play important roles in the formation of SGs [2], while RNAs are thought to act as scaffolds to bind RBPs and thus to regulate SG assembly. It has been reported that GIRGL lncRNA interacts with CAPRIN1 to drive SG formation [21]. As SG-enriched circRNAs exhibit higher ability of binding SG-related RBPs, *e.g.*, G3BP2, these circRNAs are presumed to be related to the formation of SGs. Although it has been assumed that RNAs can be recruited to SGs through the SG-related RBPs, there is no direct evidence to support this hypothesis. Moreover, RNA translation inhibition is also reported to be relevant to SG assembly [22]. However, no translation potential was detected in SG-enriched circRNAs (Table S2), suggesting that the localization of circRNAs in SGs should not be due to translation. Although longer RNAs are more likely to enrich in SGs, we observed that SG-enriched circRNAs are shorter than SG-depleted circRNAs. According to our previous study, most of circRNAs are less than 600 nt in length [23,24]. Considering the length difference between SG-enriched and SG-depleted circRNAs is limited, it may have little effect on the SG-related RBP binding of circRNAs. It should be noted that as SGs are dynamic condensates, high speed of centrifugation may affect the stability of SGs. Some SG components with weak interactions may be missed by differential centrifugation without crosslinking. However, the internal core components in SGs are more stable [25], which can be effectively captured using the approach developed in this study.

In summary, our study provides novel insights into SG-related circRNAs through transcriptome analysis of SG cores. The ability of binding SG-related RBPs of circRNAs is related to their localization in SGs, suggesting the role of circRNAs in SG formation. Also, some SG-enriched circRNAs are differentially expressed between HCC and adjacent tissues. Further studies are still needed to elucidate the specific mechanisms and cellular consequences of circRNAs in SG formation.

Materials and methods

Cell culture and stress conditions

HCC SMMC-7721 cells were cultured in the cell culture medium containing Dulbecco's modified Eagle's medium (DMEM) (Catalog No. C11995500BT, Gibco, Carlsbad, CA), 10% fetal bovine serum (Catalog No. 10270-106, Gibco, Carlsbad, CA), and 1% penicillin-streptomycin (Catalog No. 15140-122, Gibco, Carlsbad, CA) at 37℃ and 5% CO_2. For stress experiments, cells were treated with 0.5 mM $NaAsO_2$ (Catalog No. S7400-100g, Sigma-Aldrich, Saint Louis, MO) for 1 h at 37℃ and 5% CO_2.

Isolation of SGs

Isolation of SGs was performed as described in previous studies [26]. SMMC-7721 cells were seeded on 15-cm culture dishes (Catalog No. 430599, Corning, Cambridge, MA) and grown to 80% confluence. Cell culture medium was exchanged with fresh culture medium one hour prior to the stress treatment. After treating with $NaASO_2$, cells were washed once with 1 × PBS (137 mM NaCl, 2.7 mM KCl, 10 mM Na_2HPO_4, 2 mM KH_2PO_4, and pH 7.4), collected by scraping and pelleted by centrifugalization at 1500 × g for 3 min. Cells were re-suspended in 1 ml SG lysis buffer (50 mM Tris-HCl pH 7.4, 2 mM MgOAc, 100 mM KOAc, 50 μg/ml Heparin, 0.5 mM DTT, 0.5% NP40, 1 U/μl Recombinant RNase Inhibitor (Catalog No. 2313A , Takara, Tokyo, Japan), and EDTA-free protease inhibitor cocktail tablets (Catalog No. 04693132001, Roche, Basel, Switzerland)) and passed through a 25G 5/8 needle 7 times to lyse cells. Cell debris were removed after centrifugalizing at 1000 × g for 5 min at 4℃. 50 μl of the lysate supernatant was collected to isolate total RNA or perform western blot. The remaining lysate was spun at 1,8000 × g for 20 min at 4℃ to pellet SG scores. The pellets were re-suspended by SG lysis buffer and incubated with 25 μl protein A/G magnetic beads (Catalog No. 88802, Thermo Fisher Scientific, Waltham, MA) twice for 30 min at 4℃ with gentle rotation to remove nonspecific

binding proteins. Magnetic beads were removed using a magnet. The supernatants were incubated with G3BP1 antibodies (Catalog No. 13057-2-AP, Proteintech, Rosemont, IL) for 1 h at 4℃ followed by incubating with 25 µl protein A/G magnetic beads for 3 h at 4℃ with gentle rotation. The supernatants were collected to isolate supernatant RNA or perform western blot. Beads were then washed three times with wash buffer 1 (20 mM Tris-HCl pH 8.0, 200 mM NaCl, and 1 U/µl Recombinant RNase Inhibitor), wash buffer 2 (20 mM Tris-HCl pH 8.0, 500 mM NaCl, and 1 U/µl Recombinant RNase Inhibitor), and wash buffer 3 (SG lysis buffer and 2M Urea). The beads were then eluted to acquire SG proteins or resuspended with 200 µl Proteinase K buffer (1 × TE buffer, 2 M Urea, and 1 U/µl Recombinant RNase Inhibitor) for 15 min at 37℃ and the supernatants were collected to isolate SG RNA.

RNA isolation, library construction, and RNA sequencing

RNA was isolated using TRIzol LS reagent (Catalog No. 15596026, Invitrogen, Carlsbad, CA) according to the manufacturer's protocol and was dissolved in 10 µl RNase-free water. The concentration of RNAs were assessed using Qubit (Catalog No. 2061412, Thermo Fisher Scientific, Waltham, MA).

Ribosomal RNAs were depleted using KAPA RiboErase Kit (Catalog No. 07962266001, KAPA biosystem, Wilmington, MA). cDNA libraries from 10 ng ribosomal-depleted RNA were prepared using KAPA RNA HyperPrep kit (Catalog No. 7962428001, KAPA biosystem, Wilmington, MA) according to the manufacturer's protocol. The cDNA libraries (3 from cells, 3 from SGs, and 3 from supernatants without SGs) were sequenced on the Illumina NovaSeq 6000 platform with 150 bp pair-end reads.

RNA FISH and IF

RNA FISH was performed using the biotin-labeled RNA probes in the exon junction region of mRNAs and the back-splice region of circRNAs. The sense and antisense

DNA oligos containing T7 promoters and probes were synthesized and annealed. Biotin-labeled RNA probes were transcribed from the annealed products using a HiScribe™ T7 Quick High Yield RNA Synthesis Kit (Catalog No. E2050S, NEB, Ipswich, MA) and biotin RNA labeling mix (Catalog No. 11685597910 Roche, Basel, Switzerland) according to the manufacturers' protocols. Cells were seeded on glass coverslips and grown to 60%–80% confluent. Cells were washed with 1 × PBS, fixed with 4% paraformaldehyde, and permeabilized with 0.3% Triton-X 100. The prehybridization and hybridization experiments were performed using Fluorescent In Situ Hybridization Kit (Catalog No. C10910, Ribobio, Guangzhou, China) according to the manufacturer's protocol. Signals were detected using FITC labeled anti-biotin antibody (Catalog No. ab6650, Abcam, Cambridge, UK).

For IF, the RNA probe incubated cells were blocked with 5% bovine serum albumin (BSA) (Catalog No. 36103ES25, YEASEN, Shanghai, China). Antibodies were diluted in 1 × PBS containing 0.3% Triton-X 100 and 1% BSA. Cells were incubated with mouse anti-G3BP1 (Catalog No. 66486-1-Ig, Proteintech, Rosemont, IL) primary antibody for 2 h at room temperature, followed by three times washes with 1 × PBS. Cells were then incubated with Alexa Fluor 555 goat anti-rabbit (Catalog No. 4413, Cell Signaling Technology, Beverly, MA) primary antibody for 2 h at room temperature, followed by three times washes with 1 × PBS. The nucleus was stained using Hochest33342. The cell slices were mounted and images were acquired using Olympus IX83 confocal microscope (Olympus, Tokyo, Japan).

Western blot

Protein samples were separated by sodium dodecyl sulfate-polyacrylamide gel electrophoresis and transferred onto polyvinylidene fluoride membrane (Catalog No. ISEQ00010, Millipore, Billerica, MA). The membranes were blocked with 5% nonfat dried milk in TBST buffer (10 mM Tris-HCl, 150 mM NaCl, 0.1% Tween-20, and pH 7.6) for 1h at room temperature and incubated with protein specific primary antibodies

for 1 h at room temperature, followed by three times washes with TBST buffer. The membranes were then incubated with HRP conjugated secondary antibodies, followed by three times washes with TBST buffer. The protein signals were visualized using ECL chemiluminescence reagents (Catalog No. BE6706-100, EASYBIO, Beijing, China), and images were acquired using Tanon 5200 chemiluminescent imaging system (Tanon, Shanghai, China).

Quality control of RNA-seq data

Quality control was performed using FastQC (v0.11.9), and results were aggregated and visualized using MultiQC (v1.7) [27]. Sequencing adapter and low-quality sequences were trimmed using Trim_galore (v.0.6.6) with 'stringency 6' parameter. The human ribosomal RNA (rRNA) sequences were downloaded from the NCBI Nucleotide database using keyword "\"Homo sapiens\"[Organism] AND biomol_rrna[PROP]". Trimmed reads were aligned to rRNA sequences using bowtie2 (v2.3.4.3) [28] with '--very-sensitive' parameter, and aligned reads were depleted using samtools (v1.10) [29].

RNA-seq data analysis

The reference human genome and annotation (release 19, GRCh37.p13) were downloaded from GENCODE project. CIRI2 (v2.0.6) and CIRIquant (v1.1.2) was used for detection, quantification, and differential expression of circRNA in the RNA-seq libraries [30,31]. Gene expression values were calculated using the HISAT2 (v2.1.0) and StringTie (v2.0.5) pipeline [32,33]. Gene differential expression analysis was performed using the GLM model in edgeR (v.3.26.8) package [34]. PCA was performed using sklearn.decomposition.PCA function in the scikit-learn package [35].

CircRNA characterization and RBP analysis

The full-length sequences of circRNAs were downloaded from the circAtlas (v2.0) database [36]. Only circRNAs that included in circAtlas database were kept for downstream analysis. The binding sites of human RPBs were predicted using the RBPmap (v1.2) webserver with high stringency level and conservation filter, and results were parsed using custom scripts [19]. The expression of circRNAs in HCC dataset were obtained from a previous study [31]. SG-related protein database were downloaded from PhaSepDB 2.0 [37]. GO analysis was calculated using Enrichr [38].

Data availability

The raw sequence data in this study have been deposited in the Genome Sequence Archive for Human (GSA-Human) [39,40] at the National Genomics Data Center, Beijing Institute of Genomics, Chinese Academy of Sciences (GSA: HRA001512), and are publicly accessible at https://ngdc.cncb.ac.cn/gsa.

CRediT author statement

Shuai Chen: Conceptualization, Validation, Investigation, Writing - original draft. **Jinyang Zhang:** Formal analysis, Data curation, Writing - original draft. **Fangqing Zhao:** Conceptualization, Writing - review & editing, Supervision, Project administration, Funding acquisition. All authors have read and approved the final manuscript.

Competing interests

The authors have declared no competing interests.

Acknowledgements

This work was supported by grants from the National Key R&D Program (Grant Nos. 2021YFA1300500 and 2021YFA1302000) and National Natural Science Foundation of China (Grant Nos. 32130020, 32025009, and 91940306).

ORCID

0000-0003-0133-294X (Shuai Chen)

0000-0002-5163-894X (Jinyang Zhang)

0000-0002-6216-1235 (Fangqing Zhao)

References

[1] Protter DSW, Parker R. Principles and properties of stress granules. Trends Cell Biol 2016;26:668–79.

[2] Panas MD, Ivanov P, Anderson P. Mechanistic insights into mammalian stress granule dynamics. J Cell Biol 2016;215:313–23.

[3] Mahboubi H, Stochaj U. Cytoplasmic stress granules: dynamic modulators of cell signaling and disease. Biochim Biophy Acta Mol Basis Dis 2017;1863:884–95.

[4] Chatterjee D, Chakrabarti O. Role of stress granules in modulating senescence and promoting cancer progression: special emphasis on glioma. Int J Cancer 2022;150:551–61.

[5] Dudman J, Qi X. Stress granule dysregulation in amyotrophic lateral sclerosis. Front Cell Neurosci 2020;14:598517.

[6] Kedersha NL, Gupta M, Li W, Miller I, Anderson P. RNA-binding proteins TIA-1 and TIAR link the phosphorylation of eIF-2α to the assembly of mammalian stress granules. J Cell Biol 1999;147:1431–42.

[7] Tourriere H, Chebli K, Zekri L, Courselaud B, Blanchard JM, Bertrand E, et al. The RasGAP-associated endoribonuclease G3BP assembles stress granules. J Cell Biol 2003;160:823–31.

[8] Yang PG, Mathieu C, Kolaitis RM, Zhang PP, Messing J, Yurtsever U, et al. G3BP1 is a tunable switch that triggers phase separation to assemble stress granules. Cell 2020;181:325–45.

[9] Mateju D, Eichenberger B, Voigt F, Eglinger J, Roth G, Chao JA. Single-molecule imaging reveals translation of mRNAs localized to stress granules. Cell 2020;183:1801–12.

[10] Anderson P, Kedersha N. RNA granules: post-transcriptional and epigenetic modulators of gene expression. Nat Rev Mol Cell Biol 2009;10:430–6.

[11] Khong A, Matheny T, Jain S, Mitchell SF, Wheeler JR, Parker R. The stress

granule transcriptome reveals principles of mRNA accumulation in stress granules. Mol Cell 2017;68:808–20.

[12] Vihervaara A, Mahat DB, Himanen SV, Blom MAH, Lis JT, Sistonen L. Stress-induced transcriptional memory accelerates promoter-proximal pause release and decelerates termination over mitotic divisions. Mol Cell 2021;81:1715–31.

[13] Zhang J, Chen S, Yang J, Zhao F. Accurate quantification of circular RNAs identifies extensive circular isoform switching events. Nat Commun 2020;11:90.

[14] Gao Y, Zhang J, Zhao F. Circular RNA identification based on multiple seed matching. Brief Bioinform 2018;19:803–10.

[15] Gao Y, Wang J, Zheng Y, Zhang J, Chen S, Zhao F. Comprehensive identification of internal structure and alternative splicing events in circular RNAs. Nat Commun 2016;7:12060.

[16] Gao Y, Wang J, Zhao F. CIRI: an efficient and unbiased algorithm for de novo circular RNA identification. Genome Biol 2015;16:4.

[17] Wu W, Ji P, Zhao F. CircAtlas: an integrated resource of one million highly accurate circular RNAs from 1070 vertebrate transcriptomes. Genome Biol 2020;21:101.

[18] Ji P, Wu W, Chen S, Zheng Y, Zhou L, Zhang J, et al. Expanded expression landscape and prioritization of circular RNAs in mammals. Cell Rep 2019;26:3444–60.

[19] Paz I, Kosti I, Ares M, Cline M, Mandel-Gutfreund Y. RBPmap: a web server for mapping binding sites of RNA-binding proteins. Nucleic Acids Res 2014;42:W361–7.

[20] Dolicka D, Foti M, Sobolewski C. The emerging role of stress granules in hepatocellular carcinoma. Int J Mol Sci 2021;22:9428.

[21] Wang R, Cao L, Thorne RF, Zhang XD, Li J, Shao F, et al. LncRNA GIRGL drives CAPRIN1-mediated phase separation to suppress glutaminase-1 translation under glutamine deprivation. Sci Adv 2021;7:eabe5708.

[22] Fujimura K, Sasaki AT, Anderson P. Selenite targets eIF4E-binding protein-1 to inhibit translation initiation and induce the assembly of non-canonical stress granules. Nucleic Acids Res 2012;40:8099–110.

[23] Zhang J, Hou L, Zuo Z, Ji P, Zhang X, Xue Y. Comprehensive profiling of circular RNAs with nanopore sequencing and CIRI-long. Nat Biotechnol 2021;39:836–45.

[24] Zheng Y, Ji P, Chen S, Hou L, Zhao F. Reconstruction of full-length circular RNAs enables isoform-level quantification. Genome Med 2019;11:2.

[25] Jain S, Wheeler JR, Walters RW, Agrawal A, Barsic A, Parker R. ATPase-modulated stress granules contain a diverse proteome and substructure. Cell 2016;164:487–98.

[26] Khong A, Jain S, Matheny T, Wheeler JR, Parker R. Isolation of mammalian stress granule cores for RNA-Seq analysis. Methods 2018;137:49–54.

[27] Ewels P, Magnusson M, Lundin S, Kaller M. MultiQC: summarize analysis results for multiple tools and samples in a single report. Bioinformatics 2016;32:3047–8.

[28] Langmead B, Salzberg SL. Fast gapped-read alignment with Bowtie 2. Nat Methods 2012;9:357–9.

[29] Bonfield JK, Marshall J, Danecek P, Li H, Ohan V, Whitwham A, et al. HTSlib: C library for reading/writing high-throughput sequencing data. Gigascience 2021;10: giab007.

[30] Gao Y, Zhang JY, Zhao FQ. Circular RNA identification based on multiple seed matching. Brief Bioinform 2018;19:803–10.

[31] Zhang JY, Chen S, Yang JW, Zhao FQ. Accurate quantification of circular RNAs identifies extensive circular isoform switching events. Nat Commun 2020;11:90.

[32] Kim D, Landmead B, Salzberg SL. HISAT: a fast spliced aligner with low memory requirements. Nat Methods 2015;12:357–60.

[33] Pertea M, Pertea GM, Antonescu CM, Chang TC, Mendell JT, Salzberg SL. StringTie enables improved reconstruction of a transcriptome from RNA-seq reads. Nat Biotechnol 2015;33:290–5.

[34] Robinson MD, McCarthy DJ, Smyth GK. edgeR: a Bioconductor package for differential expression analysis of digital gene expression data. Bioinformatics 2010;26:139–40.

[35] Pedregosa F, Varoquaux G, Gramfort A, Michel V, Thirion B, Grisel O, et al. Scikit-learn: Machine Learning in Python. J Mach Learn Res 2011;12:2825–30.

[36] Wu WY, Ji PF, Zhao FQ. CircAtlas: an integrated resource of one million highly accurate circular RNAs from 1070 vertebrate transcriptomes. Genome Biol 2020;21:101.

[37] You K, Huang Q, Yu C, Shen B, Sevilla C, Shi M, et al. PhaSepDB: a database of liquid-liquid phase separation related proteins. Nucleic Acids Res 2020;48:D354–9.

[38] Kuleshov MV, Jones MR, Rouillard AD, Fernandez NF, Duan Q, Wang Z, et al. Enrichr: a comprehensive gene set enrichment analysis web server 2016 update. Nucleic Acids Res 2016;44:W90–7.

[39] Zhang SS, Chen X, Chen TT, Zhu JW, Tang BX, Wang AK, et al. GSA-Human: Genome Sequence Archive for Human. Yi Chuan 2021;43:988–93.

[40] Chen T, Chen X, Zhang S, Zhu J, Tang B, Wang A, et al. The Genome Sequence Archive Family: toward explosive data growth and diverse data types. Genomics Proteomics Bioinformatics 2021. https://doi.org/10.1016/j.gpb.2021.08.001.

Figure legends

Figure 1 Screening SG-specific transcripts in SGs of SMMC-7721 cells

A. The schematic workflow of inducing, isolating, and purifying SGs and sequencing of RNAs in SGs. **B**. Immunofluorescence of SGs in control and $NaAsO_2$ stimulated cells. Scale bar, 20 μm. **C**. Western blot of SG core protein G3BP1 in SGs and supernatants. **D**. Pairwise Pearson correlation coefficients between replicates of SG purified RNAs, total RNAs, and supernatant purified RNAs. **E**. Principal components analysis of individual replicates of SG purified RNAs, total RNAs, and supernatant purified RNAs. SG, stress granules; IP, immunofluorescence; WB, western blot; PC, principal components;

Figure 2 Characterization of all types of RNAs in SGs

A. Composition of the transcriptomes of SG-RNAs, total-RNAs, and sup-RNAs. **B**. Volcano plot depicting abundance of all types of transcripts in SG-RNAs versus total-RNAs. Red and blue dots indicate RNAs that are significantly enriched or depleted in SGs, respectively. **C**. RNA fluorescence *in situ* hybridization validation of RNAs enriched in SGs (*ANKRD11* and *COL7A1*). Scale bar, 5 μm. **D**. GO analysis for SG-enriched and depleted RNAs. **E–F**. Violin plots depicting the difference in transcript length (**E**) and GC content (**F**) between all types of SG-enriched and SG-depleted RNAs. ***, $P < 0.001$.

Figure 3 Characterization of circRNAs in SGs

A. Volcano plot of circRNA abundance in SG-RNAs versus total-RNAs. Red and blue dots indicate circRNAs that are significantly enriched or depleted in SGs, respectively. *P* values were calculated using GLM test in edgeR. **B**. RNA fluorescence *in situ* hybridization validation of circRNAs enriched in SGs (*circSLTM* and *circARHGAP5*). Scale bar, 5 μm. **C–H**. Violin plots of the difference in transcript length (**C**), GC content (**D**), number of RBP types (**F**), and proportion of SG-related

RBP binding sites (**H**) between SG-enriched circRNAs and SG-depleted circRNAs, as well as the number of RBP types (**E**), and proportion of SG-related RBP binding sites (**G**) between all types of SG-enriched and SG-depleted RNAs. NS, $P > 0.05$; **, $P < 0.01$; ***, $P < 0.001$. **I**. Boxplot of the binding density of top 15 RBPs with higher binding ability to SG-enriched circRNAs. The symbols on the top shows whether these RBPs are targeted to SGs. **, $P < 0.01$; ***, $P < 0.001$.

Supplementary material

Figure S1 SG-enriched circRNAs in HCC and adjacent tissues

*, $P < 0.05$; **, $P < 0.01$; ***, $P < 0.001$.

Table S1 RNA composition, reads number, and gene number of individual replicates in the transcriptomes of SG-RNAs, total-RNAs, and sup-RNAs

Table S2 Information and translation potential of SG-enriched circRNAs

Table S3 DNA Oligos used in this study

Table S4 Antibodies used in this study

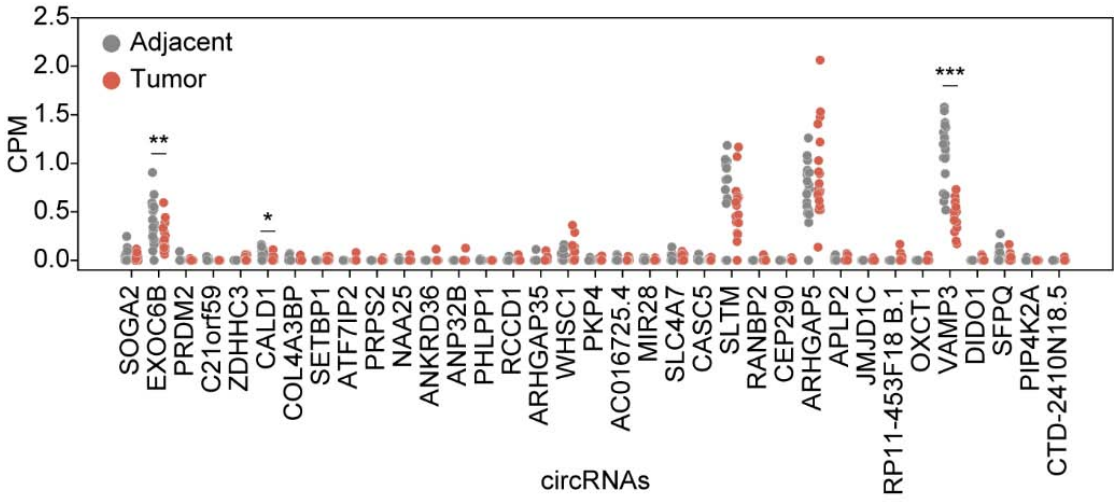

Table S1 RNA composition, reads number, and gene number of individual replicates in the transcriptomes of SG-RNAs, total-RNAs, and sup-RNAs

Gene type	Replicate	Reads number			Gene number		
		SG	Total	Sup	SG	Total	Sup
Protein coding	1	48,185,702	39,657,575	12,877,420	7249	13,404	4677
	2	45,108,953	36,583,300	40,756,487	10,916	13,349	7603
	3	84,653,437	35,192,509	38,799,786	10,332	13,287	8306
lincRNA	1	1,605,568	2,258,887	465,116	167	1479	115
	2	1,099,951	1,908,176	1,431,990	573	1399	247
	3	1,253,235	2,202,160	1,573,973	503	1399	324
Pseudogene	1	1,345,890	689,139	510,481	741	3454	705
	2	1,497,571	618,237	1,361,392	1598	3277	1224
	3	2,876,392	647,515	1,389,824	1488	3228	1404
misc RNA	1	47,942	1,217,912	26,684	23	309	31
	2	29,145	1,112,334	115,942	64	281	55
	3	48,133	852,753	98,733	67	281	67
Antisense	1	60,242	555,246	24,972	144	2063	91
	2	60,243	486,191	101,700	644	2028	234
	3	92,719	415,023	78,957	555	1968	318
Mt tRNA	1	614,877	14,759	43,723	22	21	21
	2	448,917	13,463	119,988	21	20	21
	3	862,989	18,251	110,358	21	20	21
Processed transcript	1	55,422	115,917	17,342	52	234	40
	2	40,117	100,741	58,974	125	231	78
	3	65,060	98,190	50,627	109	218	76
Sense intronic	1	11,667	52,328	12,737	34	374	34
	2	12,969	48,063	36,988	144	355	72
	3	21,171	46,772	34,796	121	358	98
circRNA	1	28,972	97,606	22,804	102	1530	88
	2	17,944	94,606	70,070	513	1483	315
	3	40,018	88,644	59,608	537	1366	410
snRNA	1	2430	28,533	1039	19	257	20
	2	1138	25,687	5105	49	238	59
	3	2242	26,694	4066	59	242	63
Sense overlapping	1	6709	16,113	2546	16	99	10
	2	6685	15,016	11,330	49	89	31
	3	10,955	14,611	7479	43	95	26
Mt rRNA	1	14,368	1024	8715	2	2	2
	2	10,758	221	12,291	2	2	2
	3	24,559	559	12,054	2	2	2
snoRNA	1	2125	20,585	3348	15	281	12
	2	2200	18,768	5334	67	275	41

	3	4053	17,991	5742	78	255	59
3' overlapping	1	1305	3233	1082	3	8	3
ncRNA	2	1082	3153	2111	7	7	2
	3	3374	3028	2427	3	8	6
miRNA	1	729	2789	373	7	91	8
	2	741	2569	1002	41	80	19
	3	953	2539	1024	35	90	18
Others	1	477	846	0	3	13	0
	2	278	781	366	6	14	2
	3	362	616	539	3	10	3
rRNA	1	105	363	295	1	14	3
	2	52	339	128	2	13	3
	3	59	308	152	4	13	5

Note: SG, stress granules.

Table S2 Information and translation potential of SG-enriched circRNAs

circRNA location	circAtlas ID	Length (nt)	GC (%)	m^6A sites	RP/PP
chr2:109369454|109389502	hsa-RANBP2_0014	341	34.90	1	0.3
chr12:88481557|88524995	hsa-CEP290_0015	75	36.00	1	0.3
chr4:1902353|1936989	hsa-WHSC1_0004	1057	48.91	0	0.3
chr11:129996595|130005610	hsa-APLP2_0001	459	51.63	1	0.3
chr20:61522312|61545758	hsa-DIDO1_0008	637	49.61	1	0
chrX:73812178|73815835	hsa-RLIM_0001	192	40.62	0	0
chr1:76253182|76259918	hsa-RABGGTB_0005	150	42.67	0	0
chr2:191300703|191302287	hsa-MFSD6_0001	1585	45.55	1	0
chr3:188326949|188426181	hsa-LPP_0001	127	52.76	1	0
chr2:234164748|234178713	hsa-ATG16L1_0003	160	48.75	1	0
chr4:7774547|7780603	hsa-AFAP1_0006	471	59.66	1	0
chr2:97856715|97877478	hsa-ANKRD36_0001	320	42.50	0	0.3
chrX:130870155|130928494	hsa-FIRRE_0016	170	44.12	0	0.3
chr15:59204762|59209198	hsa-SLTM_0001	391	37.85	0	0.3
chr3:27478879|27490288	hsa-SLC4A7_0048	286	41.96	0	0.3
chr1:7837220|7838229	hsa-VAMP3_0001	262	48.47	0	0.3
chr1:35643590|35653691	hsa-SFPQ_0006	342	48.54	0	0.3
chr2:72958136|72960247	hsa-EXOC6B_0010	412	35.92	0	0.3
chr11:103013997|103093815	hsa-DYNC2H1_0065	374	38.50	0	0
chr18:8718422|8720494	hsa-MTCL1_0002	388	48.97	0	0.3
chr1:245017620|245026032	hsa-HNRNPU_0070	186	38.17	0	0
chr7:27582586|27689252	hsa-HIBADH_0005	405	46.67	0	0
chr17:16046920|16052831	hsa-NCOR1_0033	331	39.88	0	0

chr12:22622643|22659753	hsa-C2CD5_0014	925	40.76	0	0
chr15:42736400|42738856	hsa-ZNF106_0020	131	36.64	0	0
chr15:93496587|93524687	hsa-CHD2_0130	190	38.95	0	0
chr6:44364078|44366664	hsa-CDC5L_0025	100	46.00	0	0
chr10:75299202|75336119	hsa-USP54_0076	1942	44.54	0	0
chr5:122682299|122718540	hsa-CEP120_0005	203	41.38	0	0
chr5:74698797|74706928	hsa-COL4A3BP_0027	222	41.89	0	0
chr5:41749629|41807540	hsa-OXCT1_0028	687	43.09	0	0
chr5:133493398|133510205	hsa-SKP1_0028	53	35.85	0	0
chr2:85595809|85604597	hsa-ELMOD3_0001	415	57.35	0	0
chr10:70670063|70679737	hsa-DDX50_0008	226	42.48	0	0
chr5:40746900|40747121	hsa-TTC33_0003	222	43.69	0	0
chr7:134632259|134635265	hsa-CALD1_0004	403	55.83	0	0
chr14:39870380|39871715	hsa-FBXO33_0002	111	37.84	0	0
chr15:91503130|91505004	hsa-RCCD1_0001	457	56.89	0	0
chr3:44986660|45000952	hsa-ZDHHC3_0001	557	54.76	0	0
chr10:131334505|131445098	hsa-MGMT_0013	1308	49.24	0	0
chr18:12546673|12546903	hsa-SPIRE1_0010	231	43.29	0	0
chr15:40901045|40911209	hsa-CASC5_0012	380	39.47	0	0
chr21:33979959|33982315	hsa-C21orf59_0001	313	43.45	0	0
chr10:15838099|15879317	hsa-FAM188A_0040	339	38.35	0	0
chr14:90446884|90451554	hsa-TDP1_0014	340	43.53	0	0
chr12:112515992|112516545	hsa-NAA25_0020	554	38.09	0	0
chr11:117206321|117209384	hsa-CEP164_0007	179	46.93	0	0
chrX:12817326|12828265	hsa-PRPS2_0001	408	50.25	0	0
chr18:60608951|60630705	hsa-PHLPP1_0001	437	47.83	0	0
chr11:65272291|65272490	hsa-MALAT1_0018	200	40.50	0	0
chr2:114688878|114699936	hsa-ACTR3_0011	174	34.48	0	0
chr2:159477502|159477933	hsa-PKP4_0001	323	45.82	0	0
chr10:22856780|22880710	hsa-PIP4K2A_0003	381	45.67	0	0
chr2:26346852|26350820	hsa-RAB10_0009	257	38.13	0	0
chr16:10508431|10534319	hsa-ATF7IP2_0024	455	40.66	1	0
chr2:135624112|135626611	hsa-CCNT2-AS1_0003	1353	44.27	0	0.3
chr9:100773595|100774754	hsa-ANP32B_0007	129	41.86	0	0
chr2:214012432|214014971	hsa-IKZF2_0007	221	48.42	0	0
chr1:1586823|1650894	hsa-RP1-283E3_0030	214	44.86	NA	NA
chr1:14095613|14109326	hsa-PRDM2_0004	167	47.31	NA	NA
chr18:42363353|42383064	hsa-SETBP1_0015	140	36.43	NA	NA
chr15:68476357|68479011	hsa-PIAS1_0040	979	41.06	NA	NA
chr19:47421745|47492932	hsa-CTD-2233K9_0001	355	50.42	NA	NA
chr14:32559708|32563592	hsa-ARHGAP5_0003	545	37.06	NA	NA
chr10:64936057|64937616	hsa-JMJD1C_0015	669	38.42	NA	NA

chr6:90959408|90962309	hsa-BACH2_0013	246	44.31	NA	NA

Note: RP/PP, ribosome profiling and polysome profiling evidence.

Table S3 DNA Oligos used in this study

Oligo name	Sequence
T7- circARHGAP5-prob-F	TGTAATACGACTCACTATAGGGGATCATCTTCCTTTTTATCT
T7- circARHGAP5-prob-R	AGATAAAAAGGAAGATGATCCCCTATAGTGAGTCGTATTACA
T7- circSLTM-prob-F	TGTAATACGACTCACTATAGGGTGTTTTTTACTTGGGCTGTT
T7- circSLTM-prob-R	AACAGCCCAAGTAAAAAACACCCTATAGTGAGTCGTATTACA
T7- COL7A1-prob-F	TGTAATACGACTCACTATAGGGTCTCCAACTTCACCATCTC
T7- COL7A1-prob-R	GAGATGGTGAAGTTGGAGACCCTATAGTGAGTCGTATTACA
T7- ANKRD11-prob-F	TGTAATACGACTCACTATAGGGGGGCTGTATATATTATGTC
T7- ANKRD11-prob-R	GACATAATATATACAGCCCCCCTATAGTGAGTCGTATTACA

Table S4 Antibodies used in this study

Antibody name	Company	Catalog number
G3BP1	Proteintech	13057-2-AP
G3BP1	Proteintech	66486-1-AP
GAPDH	EASYBIO	BE0023
Anti-Mouse IgG-HRP conjugated	EASYBIO	BE0102
Anti-Rabbit IgG-HRP conjugated	EASYBIO	BE0101
Anti-Rabbit IgG (Alexa Fluor 555 conjugate)	Cell Signaling Technology	#4413
Anti-Biotin (FITC conjugate)	abcam	ab6650

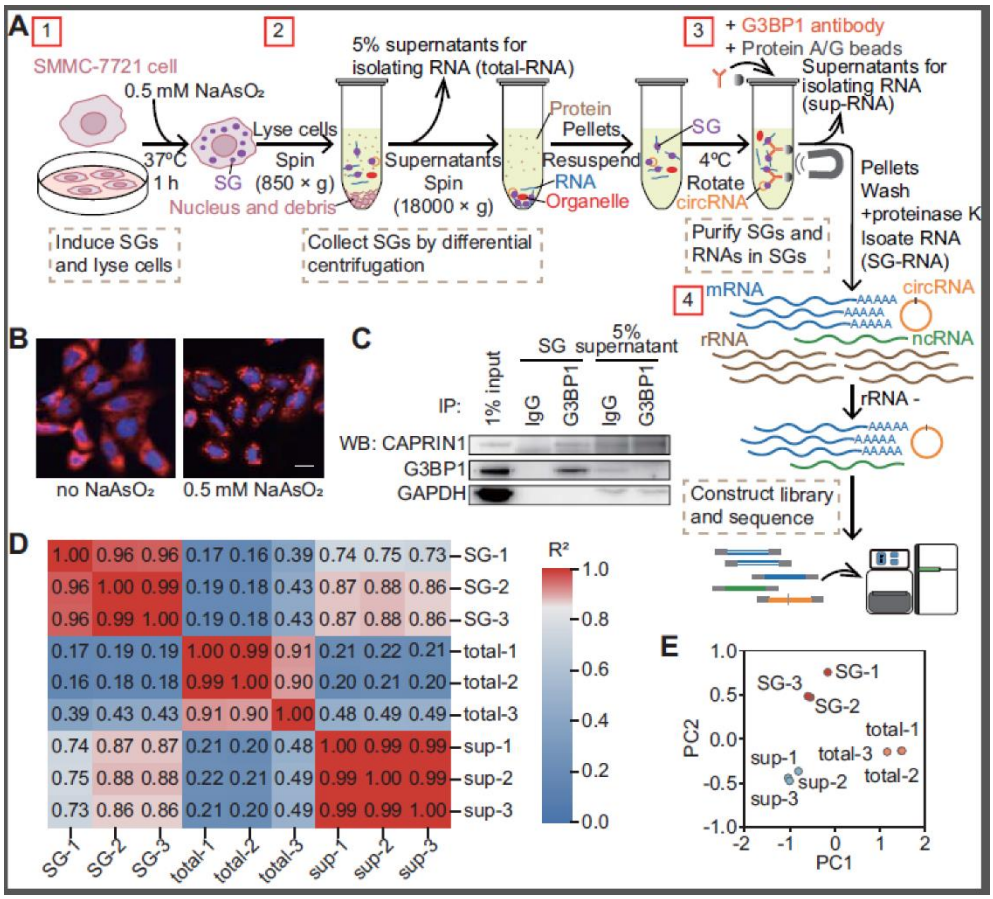
A
1
2
3
SMMC-7721 cell
0.5 mM NaAsO₂
37°C
1 h
SG
Lyse cells
Spin
(850 × g)
Nucleus and debris
5% supernatants for
isolating RNA (total-RNA)
Supernatants
Spin
(18000 × g)
Protein
Pellets
Resuspend
RNA
Organelle
SG
4°C
Rotate
circRNA
+ G3BP1 antibody
+ Protein A/G beads
Supernatants for
isolating RNA
(sup-RNA)
Pellets
Wash
+proteinase K
Isoate RNA
(SG-RNA)
Induce SGs
and lyse cells
Collect SGs by differential
centrifugation
Purify SGs and
RNAs in SGs
4
mRNA
circRNA
rRNA
ncRNA
rRNA -
Construct library
and sequence
B
no NaAsO₂
0.5 mM NaAsO₂
C
5%
SG supernatant
IP:
1% input
IgG
G3BP1
IgG
G3BP1
WB: CAPRIN1
G3BP1
GAPDH
D
1.00 0.96 0.96 0.17 0.16 0.39 0.74 0.75 0.73 SG-1
0.96 1.00 0.99 0.19 0.18 0.43 0.87 0.88 0.86 SG-2
0.96 0.99 1.00 0.19 0.18 0.43 0.87 0.88 0.86 SG-3
0.17 0.19 0.19 1.00 0.99 0.91 0.21 0.22 0.21 total-1
0.16 0.18 0.18 0.99 1.00 0.90 0.20 0.21 0.20 total-2
0.39 0.43 0.43 0.91 0.90 1.00 0.48 0.49 0.49 total-3
0.74 0.87 0.87 0.21 0.20 0.48 1.00 0.99 0.99 sup-1
0.75 0.88 0.88 0.22 0.21 0.49 0.99 1.00 0.99 sup-2
0.73 0.86 0.86 0.21 0.20 0.49 0.99 0.99 1.00 sup-3
SG-1 SG-2 SG-3 total-1 total-2 total-3 sup-1 sup-2 sup-3
R²
1.0
0.8
0.6
0.4
0.2
0.0
E
SG-1
SG-2
SG-3
total-1
total-2
total-3
sup-1
sup-2
sup-3
PC1
PC2
1.0
0.5
0.0
-0.5
-1.0
-2
-1
0
1
2

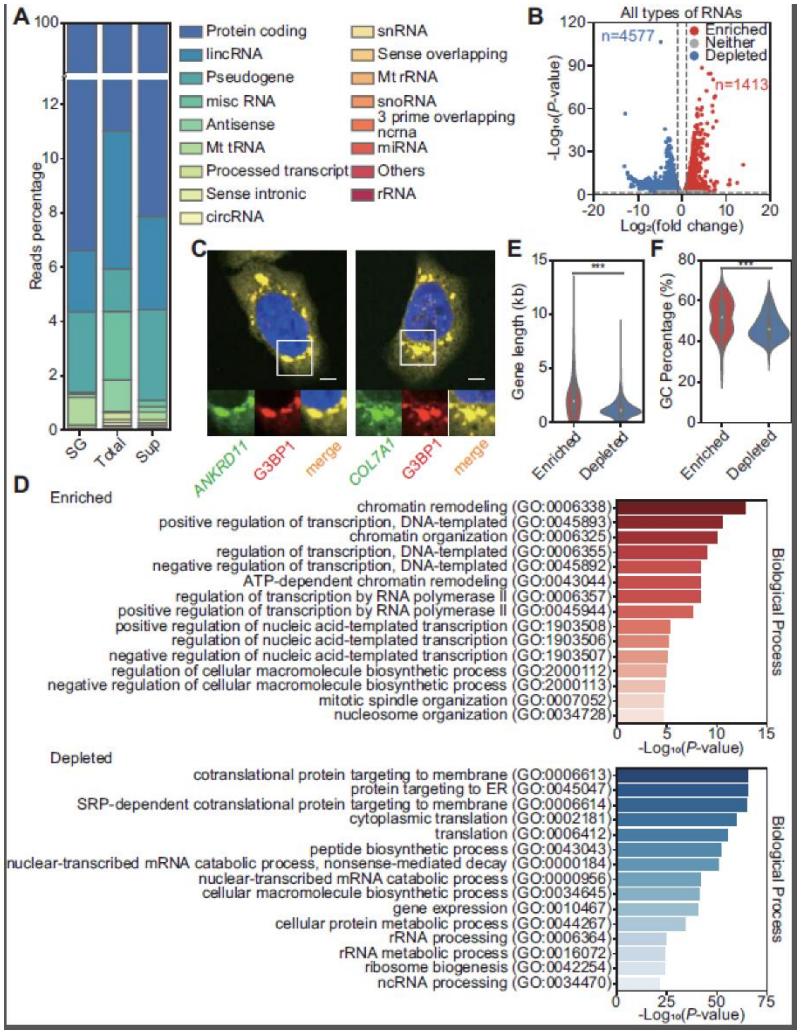
A
Reads percentage
SG
Total
Sup
Protein coding
lincRNA
Pseudogene
misc RNA
Antisense
Mt tRNA
Processed transcript
Sense intronic
circRNA
snRNA
Sense overlapping
Mt rRNA
snoRNA
3 prime overlapping ncrna
miRNA
Others
rRNA
B
All types of RNAs
n=4577
n=1413
Enriched
Neither
Depleted
-Log10(P-value)
Log2(fold change)
C
ANKRD11
G3BP1
merge
COL7A1
G3BP1
merge
E
Gene length (kb)
Enriched
Depleted
F
GC Percentage (%)
Enriched
Depleted
D
Enriched
chromatin remodeling (GO:0006338)
positive regulation of transcription, DNA-templated (GO:0045893)
chromatin organization (GO:0006325)
regulation of transcription, DNA-templated (GO:0006355)
negative regulation of transcription, DNA-templated (GO:0045892)
ATP-dependent chromatin remodeling (GO:0043044)
regulation of transcription by RNA polymerase II (GO:0006357)
positive regulation of transcription by RNA polymerase II (GO:0045944)
positive regulation of nucleic acid-templated transcription (GO:1903508)
regulation of nucleic acid-templated transcription (GO:1903506)
negative regulation of nucleic acid-templated transcription (GO:1903507)
regulation of cellular macromolecule biosynthetic process (GO:2000112)
negative regulation of cellular macromolecule biosynthetic process (GO:2000113)
mitotic spindle organization (GO:0007052)
nucleosome organization (GO:0034728)
Biological Process
-Log10(P-value)
Depleted
cotranslational protein targeting to membrane (GO:0006613)
protein targeting to ER (GO:0045047)
SRP-dependent cotranslational protein targeting to membrane (GO:0006614)
cytoplasmic translation (GO:0002181)
translation (GO:0006412)
peptide biosynthetic process (GO:0043043)
nuclear-transcribed mRNA catabolic process, nonsense-mediated decay (GO:0000184)
nuclear-transcribed mRNA catabolic process (GO:0000956)
cellular macromolecule biosynthetic process (GO:0034645)
gene expression (GO:0010467)
cellular protein metabolic process (GO:0044267)
rRNA processing (GO:0006364)
rRNA metabolic process (GO:0016072)
ribosome biogenesis (GO:0042254)
ncRNA processing (GO:0034470)
Biological Process
-Log10(P-value)

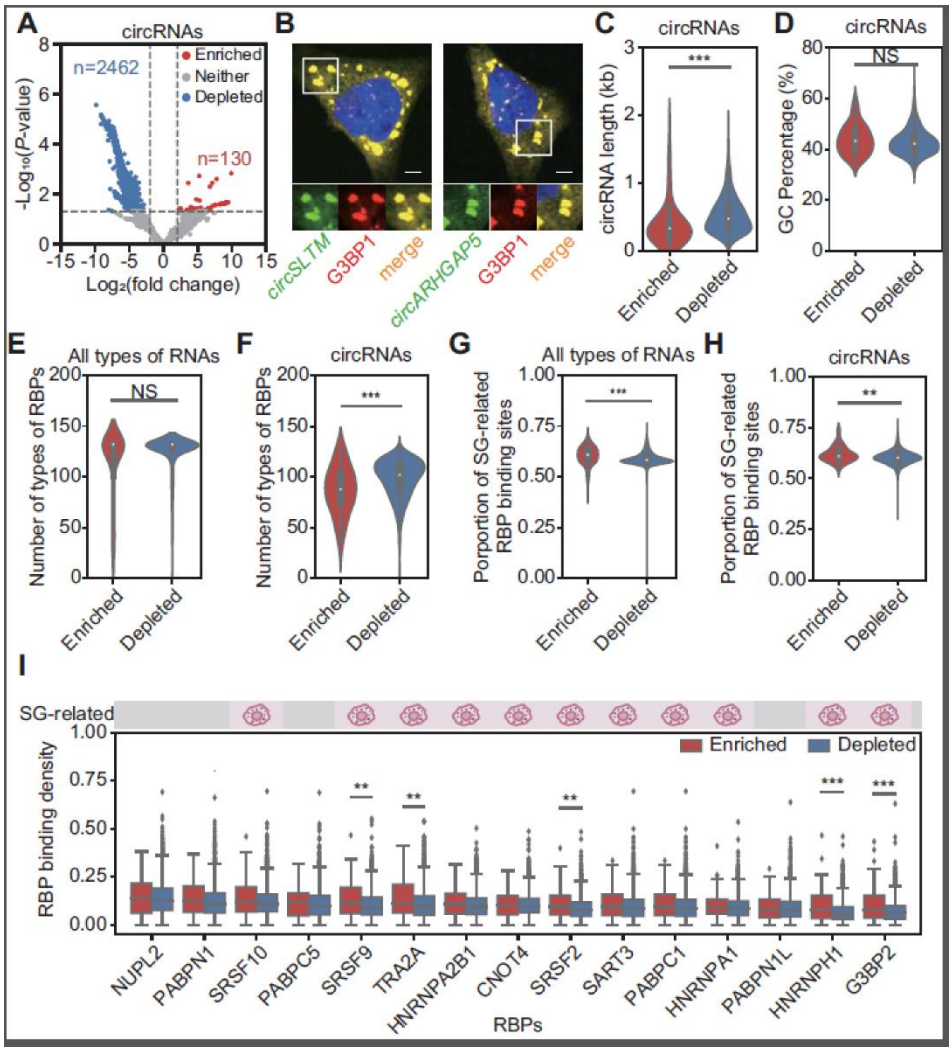
A
circRNAs
n=2462
n=130
Enriched
Neither
Depleted
-Log10(P-value)
Log2(fold change)
B
circSLTM
G3BP1
merge
circARHGAP5
G3BP1
merge
C
circRNAs
circRNA length (kb)
Enriched
Depleted
D
circRNAs
NS
GC Percentage (%)
Enriched
Depleted
E
All types of RNAs
NS
Number of types of RBPs
Enriched
Depleted
F
circRNAs
Number of types of RBPs
Enriched
Depleted
G
All types of RNAs
Porportion of SG-related RBP binding sites
Enriched
Depleted
H
circRNAs
Porportion of SG-related RBP binding sites
Enriched
Depleted
I
SG-related
Enriched
Depleted
RBP binding density
NUPL2
PABPN1
SRSF10
PABPC5
SRSF9
TRA2A
HNRNPA2B1
CNOT4
SRSF2
SART3
PABPC1
HNRNPA1
PABPN1L
HNRNPH1
G3BP2
RBPs